applied sciences

MDPI

Article

The Generalized Mohr-Coulomb Failure Criterion

Dongshuai Tian * and Hong Zheng

Key Laboratory of Urban Security and Disaster Engineering, Ministry of Education, Beijing University of Technology, Beijing 100124, China
* Correspondence: tiandongshuai@emails.bjut.edu.cn

Abstract: With the construction of supertall buildings such as high earth dams, the linear envelope of the Mohr-Coulomb (M-C) failure criterion fitted to lower confined pressure would significantly underestimate the loading capacity of foundations, causing a huge increase in the amount of earthwork. Given that the M-C criterion has dominated in the stability analysis of geotechnical structures, it is proposed in this study that the M-C criterion remain invariant in form but the cohesion c and the frictional factor f be related to the coefficient of intermediate principal stress b, called the Generalized Mohr-Coulomb (GMC) criterion. In other words, c and f are both functions of b, written as $c(b)$ and $f(b)$. In the simplest way, the GMC criterion for soils, a true three-dimensional failure criterion, can be established by using a piece of conventional triaxial apparatus. The GMC has a non-smooth strength surface like its conventional version. However, we prove from true triaxial tests and the characteristic theory of stress tensors that the failure surfaces in the stress space should be non-smooth per se for $b = 0$ or 1. Comparisons with other prominent failure criteria indicate that the GMC fits the test data best.

Keywords: failure criterion; Mohr-Coulomb failure criterion; Lade–Duncan failure criterion; SMP failure criterion; non-smooth strength surface

check for updates

Citation: Tian, D.; Zheng, H. The Generalized Mohr-Coulomb Failure Criterion. *Appl. Sci.* **2023**, *13*, 5405. https://doi.org/10.3390/app13095405

Academic Editor: Tiago Miranda

Received: 12 April 2023
Revised: 24 April 2023
Accepted: 25 April 2023
Published: 26 April 2023

Copyright: © 2023 by the authors. Licensee MDPI, Basel, Switzerland. This article is an open access article distributed under the terms and conditions of the Creative Commons Attribution (CC BY) license (https://creativecommons.org/licenses/by/4.0/).

1. Introduction

Currently, strength evaluation and deformation calculation are still the two most important problems in geotechnical engineering, as in Taylor's age [1]. For most geotechnical engineers, the phrase "strength of soils" conjures up images of Mohr-Coulomb (M-C) failure criteria [2]. Consequently, whenever new geotechnical materials are encountered, such as vegetated soil [3], lime–cement-improved clay [4], and steel slag aggregate [5], the models for evaluation of their shear strength are consistently established as close as possible to the M-C criterion.

The requirements for failure criteria in strength problems differ significantly from those in deformation problems. In the solution of strength problems, such as the stability analysis of slopes [6], the earth pressure evaluation of retaining walls [7], and the loading capacity calculation of ground foundations [8], the shear strength is the most important quantity. Hence, it is better for the shear strength to be easily derived from the failure criterion, and the M-C criterion is such a criterion that directly gives the shear strength. This might explain why the M-C criterion has been dominant in the solution of strength problems.

In the solution of deformation problems, on the other hand, a failure criterion is deemed better if the failure surface in the stress space is smooth, because the derivatives of the yield function are needed if plastic deformation is involved. From this perspective, the Lade–Duncan (L-D) criterion [9] and the SMP criterion [10] are more favorable than the M-C criterion because the M-C failure surface is not smooth in the stress space. According to the algorithms recently developed in Zheng et al. [11,12], however, non-smooth yield surfaces bring no troubles to the update of stresses in the analysis of elastic–plastic deformation.

Over the past decades, pursuing smooth yield surfaces and reflecting the influence of the intermediate stress σ_2 on failure might be two agents in developing failure criteria. The

Zienkiewicz–Pande criterion [13] and the Menetrey–Willam criterion [14] were derived by smoothing the M-C criterion. The Hoek–Brown criterion [15] does not pursue agreement with the M-C criterion, and has a smooth failure surface but does not reflect the effect of σ_2 on shear strength. Moreover, the Hoek–Brown criterion has no explicit expression of shear strength. Hence, Yang and Yin developed a "Generalized Tangential" technique in the upper bound solution for ultimate bearing capacity with the modified Hoek–Brown failure criterion [16].

To reflect the influence of σ_2 on strength, the concept of the spatially mobilized plane (SMP) was introduced by Matsuoka and Nakai [10], and they set up the SMP criterion that is expressed in terms of the three stress invariants to model the three-dimensional strength of geomaterials under different loading conditions. Meanwhile, the Lade–Duncan criterion was developed in terms of the first and the third stress invariants to model the three-dimensional strength of geomaterials based on the true triaxial compression tests of cohesionless soils [9]. The original versions of both the L-D and SMP criteria assume no cohesion, making them only applicable to sands and normally consolidated clays. The Drucker–Prager criterion, albeit commonly used, is a rather coarse approximation to the M-C criterion and inconsistent with actual cases of soils [17].

Several other failure criteria, for example, You [18], Liao et al. [19], Meyer and Labuz [20], Gao et al. [21], Li et al. [22], Liu et al. [23], and so on, have been proposed in terms of principal stresses to reflect the effect of σ_2. However, according to comparative studies in Yu et al. [24], Lu [25], Benz and Schwab [26], and Priest [27], none of the existing failure criteria has a significant advantage over the others in both mechanical mechanism and mathematical form. Thus, there are practical needs to establish a new failure criterion for the analysis of strength problems and deformation problems in geotechnical engineering.

The M-C failure criterion is widely used in geotechnical engineering because of its practicality, simple expression, and strength parameters that have physical significance and are easy to obtain using in situ or laboratory tests. However, it neglects the effect of σ_2. In fact, the influence of σ_2 on the failure behavior of geomaterials is important during engineering construction where high stress might be created [28].

In this study, we generalize the M-C criterion by simply regarding its parameters of cohesion c and friction factor f as the functions of the coefficient b of the intermediate principal stress, written as $c(b)$ and $f(b)$, respectively. Functions $c(b)$ and $f(b)$ can be obtained simply by the Lagrange interpolation or any other data fitting techniques to a series of c_i and f_i measured under different b_i. In this way, the effect of σ_2 can be naturally reflected in the failure criterion. In the simplest case, conventional triaxial tests are enough to establish a true triaxial failure criterion by linearly interpolating (c_0, f_0) measured at $b = 0$ (triaxial compression) and (c_1, f_1) at $b = 1$ (triaxial extension), which will be expounded upon shortly.

Like its classical version, the generalized M-C criterion has a non-smooth failure surface. However, we believe this is just the nature of geomaterials, and prove from true triaxial tests and the characteristic theory of stress tensors that even for isotropic geomaterial, the yield locus should be non-smooth per se in the state of $\sigma_1 \geq \sigma_2 = \sigma_3$ ($b = 0$) or $\sigma_1 = \sigma_2 \geq \sigma_3$ ($b = 1$). The authors are conscious that this is not in agreement with the "consensus" and are prepared for being questioned. The existing literature, such as Davis and Selvadurai [29] and Chen [30], claims without rigorous proof that the failure surfaces of isotropic geomaterials are smooth.

By comparing the proposed failure criterion with those celebrated failure criteria on the experimental data in the literature, it is demonstrated that the predictions by the proposed criterion agree best with experimental results.

2. Mohr-Coulomb Failure Criterion

The M-C failure criterion states that the shear strength τ_f of an isotropic geomaterial is related to the normal stress σ_n applied on the failure plane with the normal n by

$$\tau_f = c + f\sigma_n \tag{1}$$

where c is cohesion; the friction factor is $f = \tan\phi$, and ϕ is the frictional angle.

At failure, $\left(\tau_f, \sigma_n\right)$ and the principal stresses $(\sigma_1, \sigma_2, \sigma_3)$ are related by

$$\sigma_n = \frac{1}{2}(\sigma_1 + \sigma_3) - \frac{1}{2}(\sigma_1 - \sigma_3)\sin\phi \tag{2}$$

and

$$\tau_f = \frac{1}{2}(\sigma_1 - \sigma_3)\cos\phi \tag{3}$$

where σ_1 is the maximum principal stress and σ_3 is the minimum principal stress at failure. In this study, compressive stresses are designated positive.

The substitution of Equations (2) and (3) into Equation (1) leads to the M-C criterion in terms of σ_1 and σ_3

$$(\sigma_1 - \sigma_3) - (\sigma_1 + \sigma_3)\sin\phi - 2c\cos\phi = 0 \tag{4}$$

The M-C failure criterion expressed in the Mohr stress space, namely, Equation (1), is usually applied to the strength problems, such as the slope stability analysis and the computation of lateral earth pressure on retaining walls, in the framework of the limit equilibrium method [31]. The M-C criterion expressed in the stress space, namely, Equation (4), is usually applied to the deformation analysis problems [11]. Based on the assumption of elastic perfectly plasticity, in principle, a strength problem can be solved through the deformation analysis by monotonously increasing external loads [32] or consecutively reducing the strength parameters until the limit equilibrium state [33] is reached.

In order to conveniently determine the strength parameters of c and ϕ, Equation (4) is rewritten as

$$\sigma_1 - \sigma_3 = k\sigma_3 + d \tag{5}$$

where

$$k = \frac{2\sin\phi}{1 - \sin\phi} \tag{6}$$

and

$$d = 2c\cos\phi \tag{7}$$

Equation (5) depicts a straight line in the plane of σ_3~$(\sigma_1 - \sigma_3)$. The parameters of k and d can be determined simply from a series of data $\left(\sigma_1^j, \sigma_3^j\right)$, $j = 1, 2, \cdots$, from conventional triaxial tests, by applying the least squares method, say, as shown in Figure 1, with the superscript j denoting the j-th result.

For conventional triaxial compression tests, $\sigma_1^j = \sigma_a^j$, $\sigma_2^j = \sigma_3^j = \sigma_r^j$; for conventional triaxial extension tests, $\sigma_1^j = \sigma_2^j = \sigma_r^j$, $\sigma_3^j = \sigma_a^j > 0$. Here, σ_a^j and σ_r^j are the axial stress and the radial pressure of the j-th measurement at failure, respectively.

Once the parameters of k and d are derived from the above procedure, the shear strength parameters of c and ϕ can be obtained by

$$\sin\phi = \frac{k}{2 + k} \tag{8}$$

and

$$c = \frac{d}{2\cos\phi} \tag{9}$$

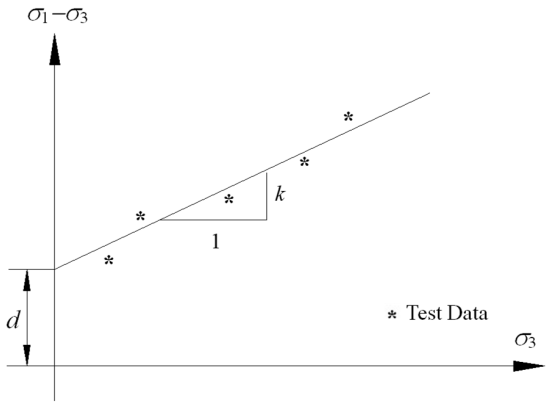


Figure 1. Mohr-Coulomb's envelope in the space of σ_3~$(\sigma_1 - \sigma_3)$.

3. The Generalized Mohr-Coulomb Criterion

The M-C criterion assumes that the effect of the intermediate principal stress σ_2 on the shear strength is negligible. However, it has been repeatedly confirmed that this is not always the case.

In order to reflect the influence of σ_2 on shear strength, we assume the M-C criterion still holds in form, but cohesion c and friction factor f are related to the coefficient b of the intermediate principal stress by

$$c_b = c(b)$$

and

$$f_b = f(b)$$

respectively, with b being the coefficient of the intermediate principal stress, defined as

$$b = \frac{(\sigma_2 - \sigma_3)}{(\sigma_1 - \sigma_3)} \tag{10}$$

Since $\sigma_1 \geq \sigma_2 \geq \sigma_3$ is specified, we have $0 \leq b \leq 1$.

As a result, the generalized Mohr-Coulomb criterion (GMC) takes form in the Mohr stress space.

$$\tau_f = c(b) + f(b)\sigma_n \tag{11}$$

From the perspective of differential geometry, the strength envelope defined by Equation (11) is a ruled surface [34] in the generalized Mohr stress space of $(\sigma, \tau; b)$, with the line

$$\begin{cases} \sigma = 0 \\ \tau = c(b) \end{cases} \tag{12}$$

being a direction of the surface; and

$$\begin{cases} \tau = c(b) \\ b = \text{const} \end{cases} \tag{13}$$

being one of the rulings. Figure 2 illustrates a GMC surface in the generalized Mohr stress space of $(\sigma, \tau; b)$.

Similarly, we have the failure locus of the GMC in the principal stress space

$$(\sigma_1 - \sigma_3) - (\sigma_1 + \sigma_3)\sin\phi(b) - 2c(b)\cos\phi(b) = 0 \tag{14}$$

with $\phi(b) = \text{tg}^{-1} f(b)$.

The simplest way to obtain functions $c(b)$ and $\phi(b)$ is to apply the Lagrange interpolation to a series of data, $(c_i, f_i; b_i)$, $i = 1, \cdots$, with $f_i = \text{tg}\phi_i$, which are based on conventional or true triaxial tests and calculated using Equations (8) and (9).

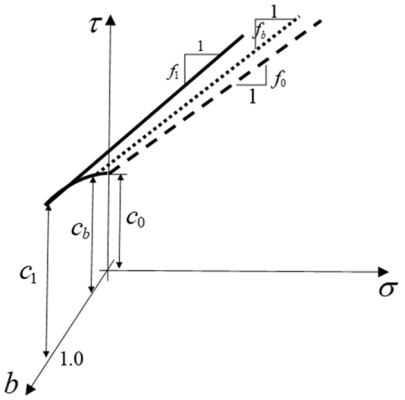


Figure 2. Illustration of GMC surface in generalized Mohr stress space of $(\sigma, \tau; b)$.

Particularly, we can interpolate the shear strength parameters of (c_0, f_0) measured from the conventional triaxial compression test ($b = 0$), and (c_0, f_0) from the conventional triaxial extension ($b = 1$) to obtain $c(b)$ and $\phi(b)$, reading

$$c(b) = c_0 L_0(b) + c_1 L_1(b) \tag{15}$$

and

$$f(b) = f_0 L_0(b) + f_1 L_1(b) \tag{16}$$

where $L_0(b)$ and $L_1(b)$ are the linear Lagrange interpolation functions, i.e.,

$$L_0(b) = 1 - b,\ L_1(b) = b \tag{17}$$

In this way, only a piece of conventional triaxial test apparatus is adequate to develop a three-dimensional failure criterion that considers the effect of σ_2. Even so, we will see shortly the GMC performs better than those celebrated failure criteria, and denote by GMC-L the GMC corresponding to (c, f) obtained by the liner Lagrange interpolation.

Similarly, the GMC corresponding to the quadric Lagrange interpolation to c and f is represented by GMC-Q, namely,

$$c(b) = \sum_{k=1}^{3} c_k L_k(b) \tag{18}$$

and

$$f(b) = \sum_{k=1}^{3} f_k L_k(b) \tag{19}$$

where (c_k, f_k), $k = 1, 2, 3$, are shear strength parameters corresponding to b_k, and L_k quadric Lagrange interpolation functions, defined by

$L_1(b) = \frac{(b-b_2)(b-b_3)}{(b_1-b_2)(b_1-b_3)}$, $L_2(b) = \frac{(b-b_3)(b-b_1)}{(b_2-b_3)(b_2-b_1)}$, and $L_3(b) = \frac{(b-b_1)(b-b_2)}{(b_3-b_1)(b_3-b_2)}$.

Here, $b_1 = 0$, $0 < b_2 < 1$, and $b_3 = 1$ are the most selected for b_k.

Figure 3 shows the surfaces of the M-C and the GMC on the π plane corresponding to some mean pressure $p(= I_1/3)$, respectively, suggesting that the GMC surface contains the M-C surface, but coincides with the M-C surface at vertex A ($b = 0$). In general, the intersection of the GMC surface is defined by Equation (14) and the plane of b = constant, i.e.,

$$b = \frac{\sigma_2 - \sigma_3}{\sigma_1 - \sigma_3} = \text{constant}$$

is a meridian line, which is a straight line in the principal stress space because b uniquely determines the values of $c(b)$ and $\phi(b)$ in Equation (14).

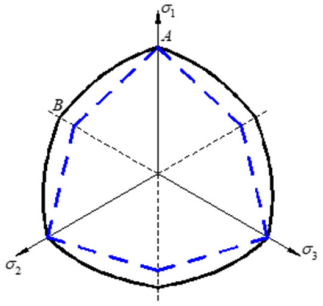


Figure 3. Inner M-C and outside GMC yield loci on π plane.

Figure 4 displays the images of the M-C surface and the GMC-Q surface in the principal stress space that have the same c_0 and f_0, indicating that the M-C surface is contained in the GMC surface and the same meridian line of $b = 0$ is shared by the two surfaces.

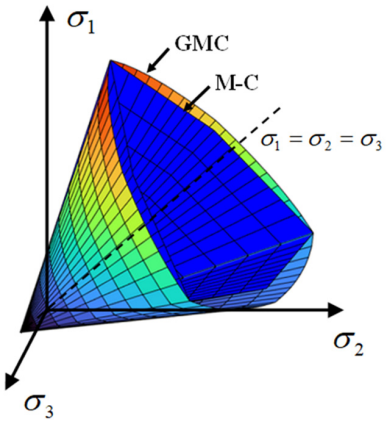


Figure 4. Images of M-C and GMC.

Figure 5 displays the shear strength τ_f evaluated by GMC-L according to some true triaxial tests from the literature [35–42], which suggests that for each fixed σ_3, τ_f increases as b increases.

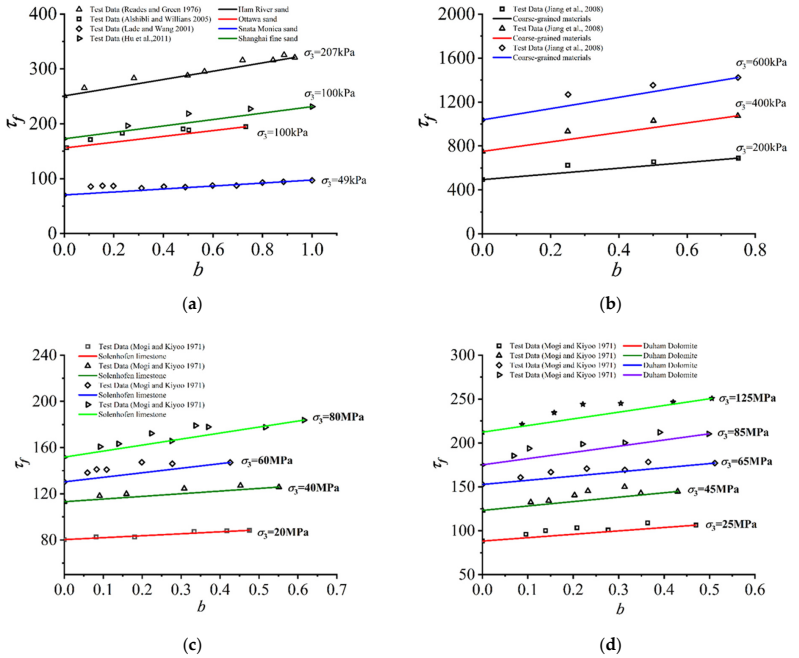


Figure 5. *Cont.*

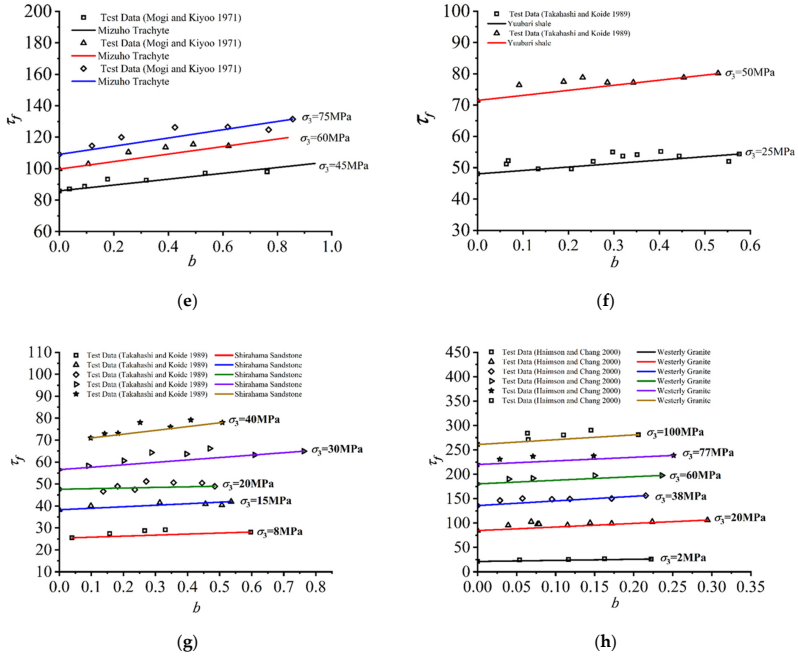


Figure 5. Relationships between shear strength τ_f and b of some geomaterials with different σ_3 using GMC-L (**a**) Geotechnical materials [35–38]; (**b**) Coarse-grained materials [39]; (**c**) Solenhofen limestone [40]; (**d**) Duham dolomite [40]; (**e**) Mizuho trachyte [40]; (**f**) Yuubari shale [41]; (**g**) Shirahama sandstone [41]; (**h**) Westerly granite [42].

4. The Justification of GMC

The GMC expressed in the Mohr stress space, i.e., Equation (11), is based on two facts. Firstly, the failure of geomaterials belongs to shear failure, and the shear strength comes from the cohesion and the friction strength. Secondly, according to laboratory tests, including direct shear tests and conventional triaxial tests, shear strength decreases as σ_2 approaches σ_3 and reaches the minimum while $\sigma_2 = \sigma_3$ or $b = 0$, while shear strength increases as σ_2 exceeds σ_3.

In the case of dense sands, for example, it has been shown in Craig [43] that the peak value of ϕ in plane strain ($b > 0$) can be 4° or 5° higher than the corresponding value obtained by conventional triaxial compression ($b = 0$). In the case of clays, for another example [2], friction angles in plane strain ($b > 0$) are typically 10 percent higher than that in conventional triaxial compression ($b = 0$). These facts lead us to conclude that the friction factor f is a function of b, denoted by f(b).

Just recently, Rosales Garzón and Hanna [44] did an in-depth study on mechanism that the plane–strain frictional angle developed by cohesionless soils is above the conventional triaxial compression frictional angle.

It can be justified that the cohesion c is also a function of b, written as $c(b)$. Here is a deduction for overconsolidated clays in conventional triaxial compression.

According to the critical state theory [8], the state (p, q, v) of an overconsolidated clay element in the peak strength is on the Hvorslev surface with the equation

$$q = (M - m) \exp \frac{\Gamma - v}{\lambda} + mp \tag{20}$$

Here, q is known as the deviator stress, defined by $q = \sigma_1 - \sigma_3$; p as the mean stress, by $p = \frac{1}{3}(\sigma_1 + 2\sigma_3)$; and v as the specific volume, by $v = 1 + e$ with e the void ratio. In Equation (20), M, m, λ, and Γ are mechanical constants of the clay.

The M-C criterion can also be expressed in terms of (p, q) as

$$q = \frac{6c \cos \phi}{3 - \sin \phi} + \frac{6 \sin \phi}{3 - \sin \phi} p \tag{21}$$

By comparing Equations (20) and (21), it is followed that admitting the critical state theory leads us to the conclusion that the peak friction angle ϕ is also a constant that is uniquely determined by m, and the peak cohesion c is a monotonically decreasing function of v, i.e.,

$$c = \frac{1}{3}\Lambda \exp \frac{\Gamma - v}{\lambda} \tag{22}$$

with

$$\Lambda = \frac{(M-m)(3-\sin\phi)}{6\cos\phi} \tag{23}$$

As σ_2 varies from σ_3 to σ_1, or as b increases from zero to one, the mean stress p increases from $\frac{1}{3}(\sigma_1 + 2\sigma_3)$ to $\frac{1}{3}(2\sigma_1 + \sigma_3)$, because p is related to b by

$$p \equiv \frac{1}{3}(\sigma_1 + \sigma_2 + \sigma_3) = \frac{1}{3}(\sigma_1 + 2\sigma_3) + \frac{1}{3}(\sigma_1 - \sigma_3)b$$

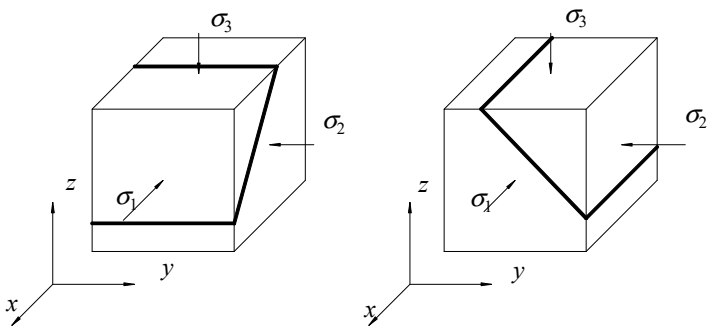
Prior to the peak strength, v is dominantly controlled by p, and hence by b. Therefore, the cohesion c is a function of b according to Equation (22). This concludes the deduction of the GMC criterion.

5. The Justification of Non-Smoothness of Failure Surfaces of Geomaterials

Like its classical version, the GMC has a non-smooth failure surface, and the failure plane takes an angle with σ_1, equaling $\pm\left(\frac{\pi}{4} - \frac{\phi}{2}\right)$. The non-smoothness of the failure surface might be deemed a drawback of the GMC. Here, we demonstrate, from true axial tests and the characteristic theory of stress tensors, respectively, that even for an isotropic geomaterial, the failure surface should be non-smooth per se.

5.1. Deduction from True Triaxial Tests

Let σ_1, σ_2, and σ_3, acting on an infinitesimal volume, be always parallel to the x, y, and z axis, respectively, as shown in Figure 6a, and let the failure of the infinitesimal volume be represented by the occurrence of plastic deformation or the shear band.



(**a**) (**b**)

Figure 6. The infinitesimal volume in the yield condition is stressed by $(\sigma_1, \sigma_2, \sigma_3)$. While the stress changes from the state of $\sigma_1 > \sigma_2 > \sigma_3$ to $\sigma_1 = \sigma_2 > \sigma_3$, the orientation of the shear band (represented by the thick lines) has an abrupt change (**a**) $\sigma_1 > \sigma_2 \geq \sigma_3$ makes failure surface parallel to the y axis; (**b**) $\sigma_1 = \sigma_2 \geq \sigma_3$, with $\dot{\sigma}_2 > 0$, makes failure surface parallel to the x axis.

Firstly, let the stress point (σ_1,σ_2,σ_3) be on the patch AB of the yield surface in Figure 3, where $\sigma_1 > \sigma_2 \geq \sigma_3$ or $0 \leq b < 1$. The yield surface AB is represented by equation

$$F(\sigma_1, \sigma_2, \sigma_3) = 0$$

Associated with the stress state of $\sigma_1 > \sigma_2 \geq \sigma_3$ is the shear band that is across the infinitesimal volume and always parallel to the y axis according to true triaxial tests and rep-

resented by the thick line, as shown in Figure 6a. Then, let the stress point (σ_1, σ_2, σ_3) move along AB (in Figure 3) by gradually increasing σ_2. During this movement, the shear band corresponding to the stress state of $\sigma_1 > \sigma_2 \geq \sigma_3$ is still parallel to the y axis until $\sigma_1 = \sigma_2 > \sigma_3$, at which the shear band has an abrupt change if σ_2 continues to increase, i.e., $\dot{\sigma}_2 > 0$, becoming parallel to the x axis, as shown in Figure 6b.

This demonstrates to us that when the stress point (σ_1, σ_2, σ_3) on the yield surface moves from point A to point B, as shown in Figure 3, satisfying $\sigma_1 > \sigma_2 \geq \sigma_3$, the shear band orientation does not change or changes little, but is always parallels to the y axis, until point B is reached, at which $\sigma_2 = \sigma_1 > \sigma_3$. According to plastic flow theory, the direction of plastic deformation, which determines the orientation of the shear band, is determined to a great degree by the gradient of the yield function,

$$\left(\frac{\partial F}{\partial \sigma_1}, \frac{\partial F}{\partial \sigma_2}, \frac{\partial F}{\partial \sigma_3}\right)$$

An abrupt change in the orientation of the shear band declares an abrupt change in the gradient of the yield function $F(\sigma_1, \sigma_2, \sigma_3)$. Therefore, the yield surface should be non-smooth at the meridian line passing the point B in Figure 3, on which $\sigma_1 = \sigma_2 > \sigma_3$ or $b = 1$.

5.2. Deduction from Characteristic Theory of Stress Tensors

Suppose the geomaterial of interest is isotropic, and accordingly, the equation of the failure surface in the stress space is still written as $F(\sigma_1, \sigma_2, \sigma_3) = 0$, where σ_k is the k-th principal stress (k = 1, 2, 3) and, in some subspace of the principal stress space, such as $\sigma_1 \geq \sigma_2 \geq \sigma_3$, regarded as the smooth function of the Voigt stress components $\sigma_{11}(=\sigma_x)$, $\sigma_{22}(=\sigma_y)$, $\sigma_{33}(=\sigma_z)$, $\sigma_{12}(=\tau_{xy})$, $\sigma_{23}(=\tau_{yz})$, and $\sigma_{31}(=\tau_{zx})$. Then, the gradient of F at the stress point σ_{ij} is

$$\frac{\partial F}{\partial \sigma_{ij}} = \sum_{k=1}^{3} \frac{\partial F}{\partial \sigma_k} \frac{\partial \sigma_k}{\partial \sigma_{ij}} \tag{24}$$

In order to calculate $\frac{\partial \sigma_k}{\partial \sigma_{ij}}$, we start from the characteristic equation of stress tensor

$$\sigma_k \boldsymbol{l}_k = \boldsymbol{S}\boldsymbol{l}_k \tag{25}$$

Here, the index k does not refer to summation; $\boldsymbol{l}_k$ is the k-th principal direction corresponding to σ_k, with $\|\boldsymbol{l}_k\|_2 = 1$; and $\boldsymbol{S}$ is the 3×3 symmetric matrix, with σ_{ij} or σ_{ji} being the components.

Premultiplying $\boldsymbol{l}_k^T$ and then differentiating with respect to σ_{ij} on both sides of Equation (25), we have

$$\frac{\partial \sigma_k}{\partial \sigma_{ij}} = \frac{\partial \boldsymbol{l}_k^T}{\partial \sigma_{ij}} \boldsymbol{S}\boldsymbol{l}_k + \boldsymbol{l}_k^T \frac{\partial \boldsymbol{S}}{\partial \sigma_{ij}} \boldsymbol{l}_k + \boldsymbol{l}_k^T S \frac{\partial \boldsymbol{l}_k}{\partial \sigma_{ij}} \tag{26}$$

Due to $\boldsymbol{S} = \boldsymbol{S}^T$, the first item on the right-hand side equals the third one, leading to

$$\frac{\partial \sigma_k}{\partial \sigma_{ij}} = 2\frac{\partial \boldsymbol{l}_k^T}{\partial \sigma_{ij}} \boldsymbol{S}\boldsymbol{l}_k + \boldsymbol{l}_k^T \frac{\partial \boldsymbol{S}}{\partial \sigma_{ij}} \boldsymbol{l}_k \tag{27}$$

The substitution of Equation (25) into Equation (27) gives rise to

$$\frac{\partial \sigma_k}{\partial \sigma_{ij}} = 2\sigma_k \frac{\partial \boldsymbol{l}_k^T}{\partial \sigma_{ij}} \boldsymbol{l}_k + \boldsymbol{l}_k^T \frac{\partial \boldsymbol{S}}{\partial \sigma_{ij}} \boldsymbol{l}_k \tag{28}$$

The first item of the right-hand side of Equation (28) vanishes due to $\boldsymbol{l}_k^T \boldsymbol{l}_k = 1$, leading to

$$\frac{\partial \sigma_k}{\partial \sigma_{ij}} = \boldsymbol{l}_k^T \frac{\partial \boldsymbol{S}}{\partial \sigma_{ij}} \boldsymbol{l}_k = (2 - \delta_{ij}) l_k^i l_k^j \tag{29}$$

where δ_{ij} is the Kronecker delta, and none of indices, i, j, or k, refers to summation; l_k^i is the i-th component of the k-th principal direction $\boldsymbol{l}_k$. It is noted that the final result of Equation (29) is derived by deeming σ_{ij} and σ_{ji} the same variable, implying that

$$\frac{\partial \boldsymbol{S}}{\partial \sigma_{22}} = \begin{bmatrix} 0 & 0 & 0 \\ 0 & 1 & 0 \\ 0 & 0 & 0 \end{bmatrix}, \frac{\partial \boldsymbol{S}}{\partial \sigma_{23}} = \begin{bmatrix} 0 & 0 & 0 \\ 0 & 0 & 1 \\ 0 & 1 & 0 \end{bmatrix}$$

and so on.

If $\sigma_1 = \sigma_2$, either $\boldsymbol{l}_1$ or $\boldsymbol{l}_2$ is indeterminant, and any two unit vectors perpendicular to each other can be $\boldsymbol{l}_1$ and $\boldsymbol{l}_2$, which are both perpendicular to $\boldsymbol{l}_3$, thereby causing the partial differentials of both $\frac{\partial \sigma_1}{\partial \sigma_{ij}}$ and $\frac{\partial \sigma_2}{\partial \sigma_{ij}}$ indeterminant. As a result, the normal vector $\frac{\partial F}{\partial \sigma_{ij}}$ of function F is also indeterminant at the state of $\sigma_1 = \sigma_2$ according to Equation (24). Once again, we prove that the yield surface is not smooth at $\sigma_1 = \sigma_2$.

As for those smooth yield criteria, such as the Mises criterion, the yield function F can be always written as a smooth function of the stress component σ_{ij} in the whole principal stress space. When finding the normal of the surface $F = 0$, it is obtained by directly finding the partial derivative of F with respect to σ_{ij}, rather than by Equation (24).

6. Comparisons with Commonly Used Failure Criteria

For geomaterials, there have been some failure criteria that consider the effect of σ_2 on shear strength [22]. In this section, we collect some test data of true triaxial tests from Reades and Green [35], Alshibli and Williams [36], Lade and Wang [37], Hu et al. [38], Jiang et al. [39], Mogi [40], Takahashi and Koide [41], Haimson and Chang [42], Sutherland and Mesdary [45], Shi et al. [46], Ma and Haimson [47], Chang and Haimson [48], and Liu [49]. Comparisons are made from the prediction capacity of both shear strength and deformation among the four failure criteria of the M-C, L-D, SMP, and the GMC.

6.1. L-D and SMP Criterion

The L-D criterion to participate in comparisons takes the form

$$\frac{I_1^3}{I_3} = k_{LD} \tag{30}$$

where

$$I_1 = \sigma_1 + \sigma_2 + \sigma_3 \tag{31}$$

and

$$I_3 = \sigma_1 \sigma_2 \sigma_3 \tag{32}$$

k_{LD} is the material constant related to the friction angle ϕ_0 associated with $b = 0$ by

$$k_{LD} = \frac{(3 - \sin\phi_0)^3}{1 - \sin\phi_0 - \sin^2\phi_0 + \sin^3\phi_0} \tag{33}$$

For $b > 0$, given by the L-D criterion is a real root of the cubic equation as follows [46]

$$\begin{aligned} &(2b-1)\left[k_{LD} + (2b-1)^2\right]\sin^3\phi_b + \left[k_{LD} + 9(2b-1)^2\right]\sin^2\phi_b \\ &+(27 - k_{LD})(2b-1)\sin\phi_b + 27 - k_{LD} = 0 \end{aligned} \tag{34}$$

The SMP criterion, as another failure criterion to participate in the comparison, takes the form

$$\frac{I_1 I_2}{I_3} = k_{SMP} \tag{35}$$

where

$$I_2 = \sigma_2\sigma_3 + \sigma_3\sigma_1 + \sigma_1\sigma_2 \tag{36}$$

k_{SMP} is the material constant defined by

$$k_{SMP} = 8\tan^2\phi_0 + 9 \tag{37}$$

For $b > 0$, given by the SMP criterion is a real root of the cubic equation as follows [46]

$$\begin{aligned}&(k_{SMP}-1)(2b-1)\sin^3\phi_b + \left[2(2b-1)^2 - 3 + k_{SMP}\right]\sin^2\phi_b \\ &+(9-k_{SMP})(2b-1)\sin\phi_b + 9 - k_{SMP} = 0\end{aligned} \tag{38}$$

As for the GMC, we emphasize again c_b and ϕ_b in the criterion are obtained by the Lagrange interpolation stated in Section 3.

6.2. Comparisons of Shear Strength

Now let us compare the capability for the four criteria of M-C, L-D, SMP, and GMC-L, respectively, to predict the shear strength.

Figure 7 illustrates the images of ϕ_b~b given by the four criteria, respectively, suggesting that:

(1) By and large, the friction angle ϕ_b from the test increases with the increase in b;
(2) The M-C criterion is accurate only under the conventional triaxial condition, underestimating the friction angle to a bigger b;
(3) The L-D criterion overestimates the contribution of b to the friction angle, particularly for $b \approx 0.4$;
(4) If $0 \leq b < 0.5$, the SMP criterion is relatively consistent with the test data, but if $0.5 \leq b \leq 1$, it underestimates the contribution of b to soil strength;
(5) The GMC-L criterion matches the test data best even if the simplest linear interpolation is employed to the data of (c_0, f_0) at $b = 0$ and (c_1, f_1) at $b = 1$. The two groups of data can be directly measured with conventional triaxial tests.

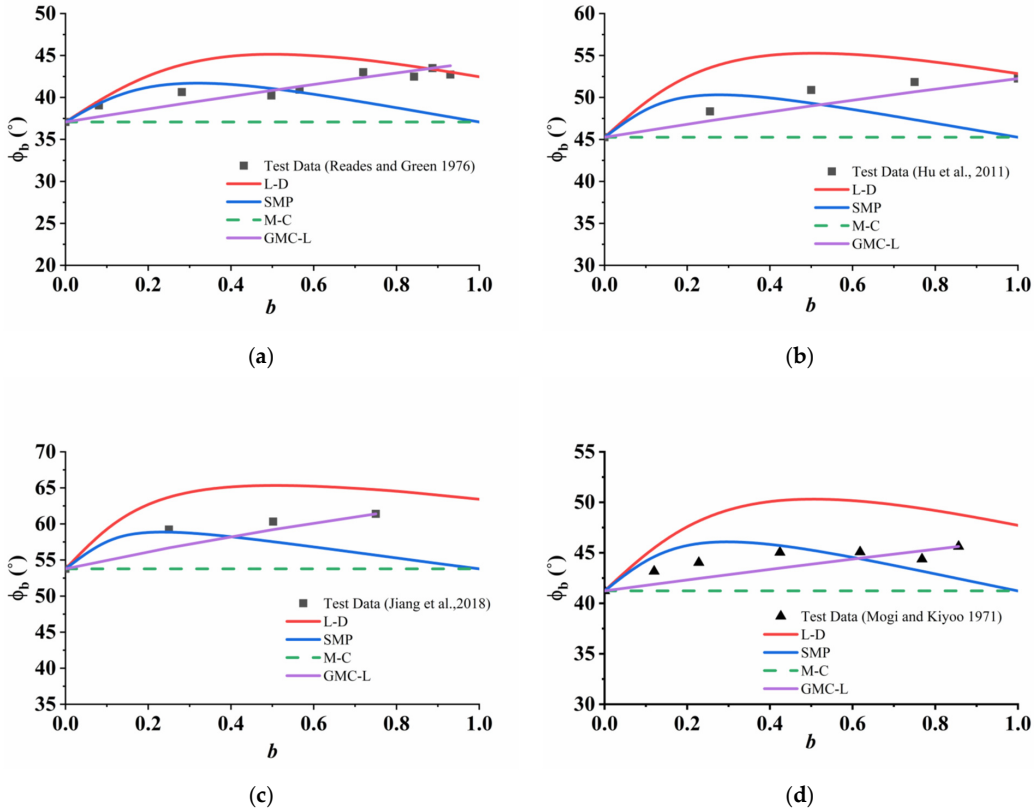


Figure 7. *Cont.*

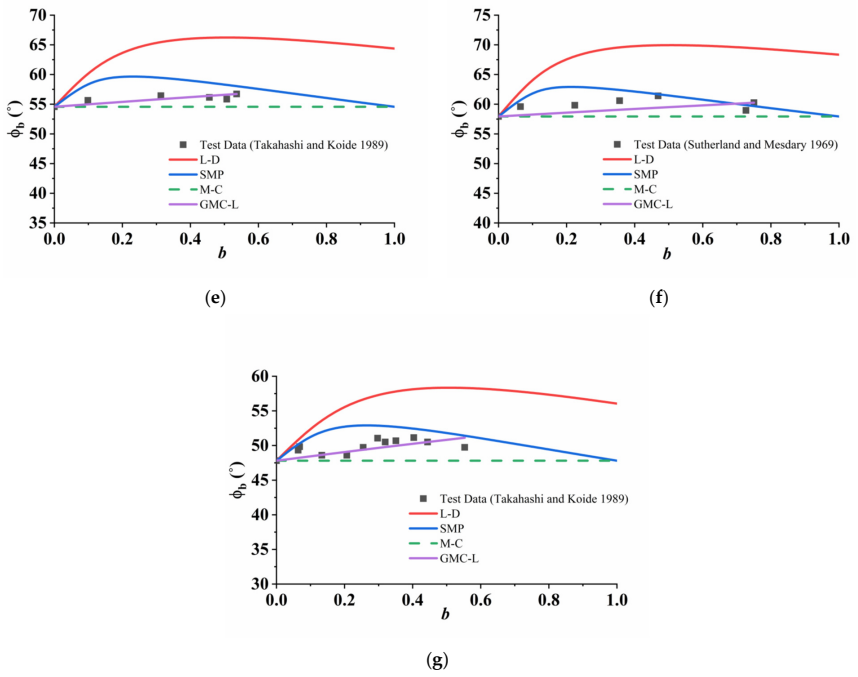


Figure 7. Relationships between friction angle ϕ_b and coefficient of intermediate principal stress b (**a**) Ham River sand [35]; (**b**) Shanghai fine sand [38]; (**c**) Coarse-grained materials (σ_3 = 200 kPa) [39]; (**d**) Mizuho trachyte (σ_3 = 75 MPa) [40]; (**e**) Shirahama sandstone [41]; (**f**) Taiwan siltstone [45]; (**g**) Yuubari shale (σ_3 = 25 MPa) [41].

Figures 8 and 9 display more images of ϕ_b by the four failure criteria, implicating that while GMC-L is not very good at fitting experimental data, GMC-Q is always able to approximate them very well.

For cohesive soil, Figure 10 shows the prediction results of GMC-L for the strength parameters of loess with different moisture contents (w), while Figure 11 shows the images of ϕ_b and c_b by using GMC-Q to some true triaxial tests from Liu [49]. From the comparisons with the experimental data, it is observed that GMC is suitable for the prediction of the cohesion as well as the friction angle.

6.3. Comparisons of Deviatoric Stress

In the above, we compared performances of the four failure criteria in the Mohr stress space, which represent the capacity for them to predict the shear strength of geomaterials.

Here, we compare the performances of the same four failure criteria in the stress space, which represent the capacity for them to predict both the shear strength and the deformation of geomaterials because the deformation analysis is usually carried out in the stress space rather than the Mohr stress space.

Let us compare the deviatoric stress q predicted by the four criteria. The square of q is defined as

$$q^2 = \frac{1}{2}\left[(\sigma_2 - \sigma_3)^2 + (\sigma_3 - \sigma_1)^2 + (\sigma_1 - \sigma_3)^2\right] \tag{39}$$

As we know, q plays the most important role in the shear deformation of geomaterials.

In calculating q in Equation (39), σ_2 and σ_3 always take values from experimental tests. The value of σ_1 has two choices: if σ_1 takes values from experimental tests, then the relevant deviatoric stress is denoted by q_T; if, otherwise, σ_1 is calculated using Equation (30) for the L-D criterion, then the relevant deviatoric stress is represented by q_{LD}. Similarly, we have the deviatoric stress q_{SMP} evaluated by the SMP criterion from Equation (35) and q_{GMC} by the GMC criterion from Equation (14).

If the difference $|q_T - q_{LD}|$ is the minimum, say, then the L-D criterion matches best with the test result.

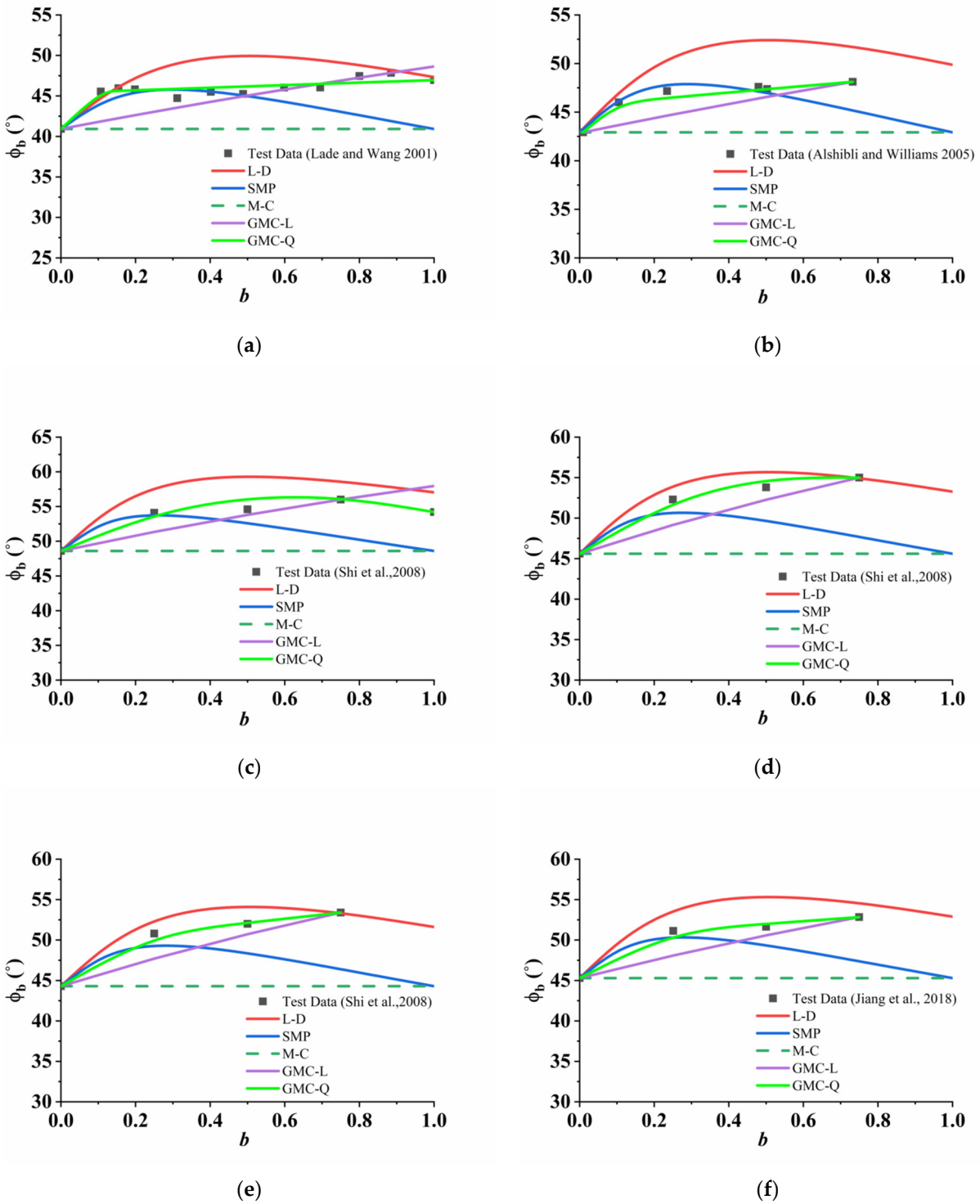


Figure 8. Relationships between friction angle ϕ_b and b for geotechnical materials (**a**) Santa Monica sand [37]; (**b**) Ottawa sand [36]; (**c**) Gravel (σ_3 = 100 kPa) [46]; (**d**) Gravel (σ_3 = 125 kPa) [46]; (**e**) Gravel (σ_3 = 150 kPa) [46]; (**f**) Coarse-grained materials (σ_3 = 600 kPa) [39].

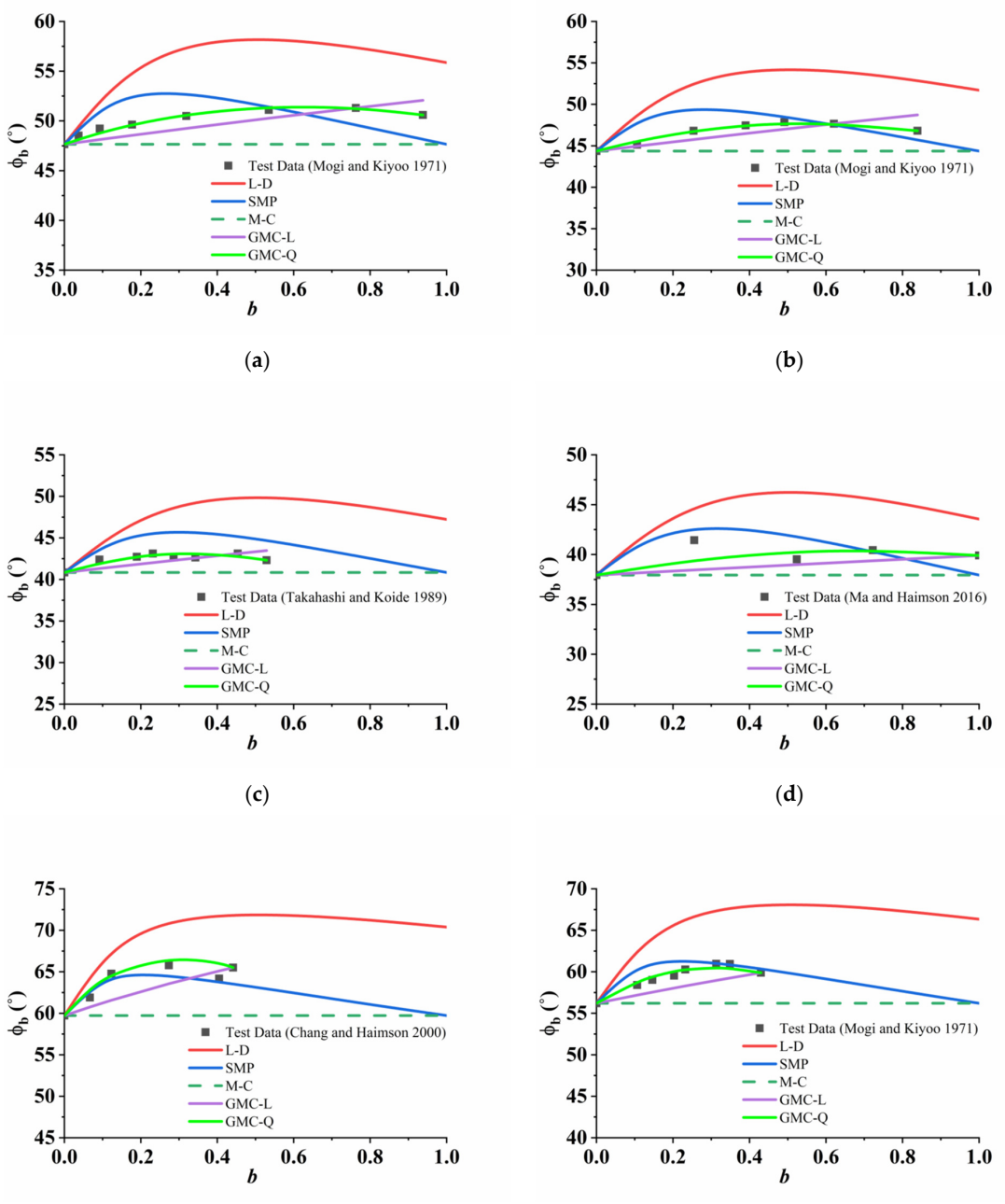


Figure 9. Relationships between friction angle ϕ_b and b for rocks: (**a**) Mizuho trachyte (σ_3 = 45 MPa) [40]; (**b**) Mizuho trachyte (σ_3 = 60 MPa) [40]; (**c**) Yuubari shale (σ_3 = 50 MPa) [41]; (**d**) Bentheim sandstone [47]; (**e**) KTB amphilolite [48]; (**f**) Dunham dolomite [40].

Figures 12 and 13 display the bar charts of the deviatoric stress q given by the four failure criteria for different σ_2. For all the cases,

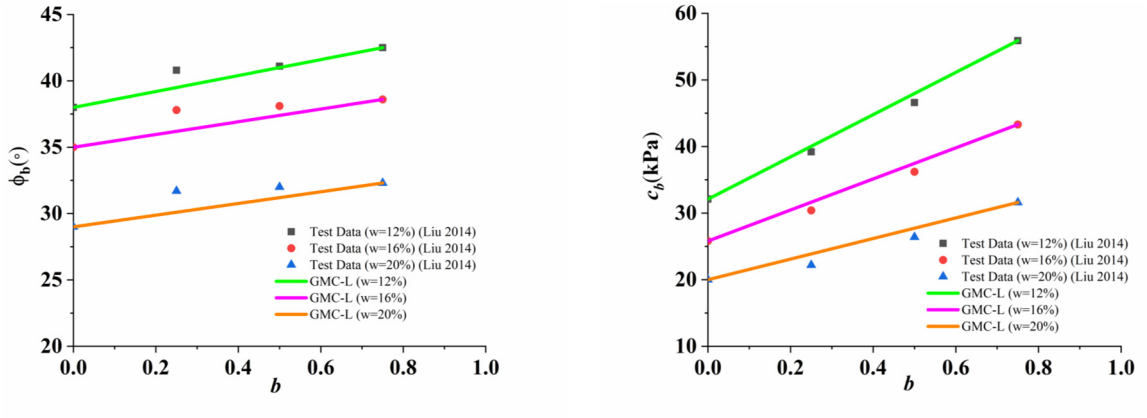
(1) GMC-Q matches best with the tests, and GMC-L second;

(2) q_{MC} is the minimum, suggesting that using the M-C criterion always overestimates the shear deformation because the geomaterial is easiest to reach the deviatoric stress strength and start plastic deformation under the same external load;

(3) q_{LD} is the maximum, implying that the application of the L-D criterion always underestimates the shear deformation because the geomaterial is hardest to reach the deviatoric stress strength and start plastic deformation under the same external load.

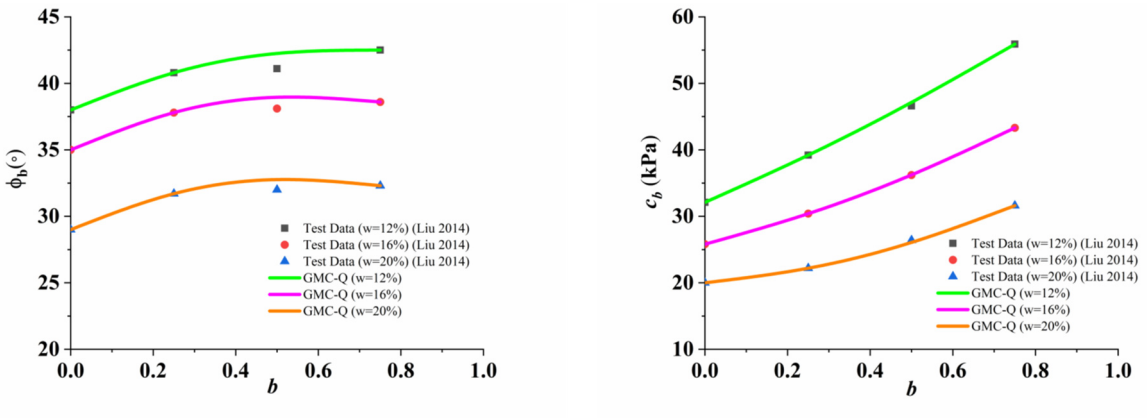
Lastly, we show in Figure 14 the comparisons in the σ_1-σ_2 plane and for some fixed σ_3 between experimental data of true triaxial tests and the predictions of L-D, SMP, and GMC-Q, respectively. It is observed that for different soils and rocks, GMC-Q is always in best agreement with the test results; meanwhile, σ_1 varies almost linearly with σ_3 by using GMC-L.

More test results have been collected and utilized to make comparisons. All the comparisons confirm without exception that GMC matches best with the experimental observations. To avoid lengthily repeating, the presentation concludes here.



(**a**) (**b**)

Figure 10. Relationships between strength parameters and coefficient of intermediate principal stress for loess [49] (**a**) Internal friction angle; (**b**) Cohesion.



(**a**) (**b**)

Figure 11. Relationships between strength parameters and b for loess [49] (**a**) Internal friction angle; (**b**) Cohesion.

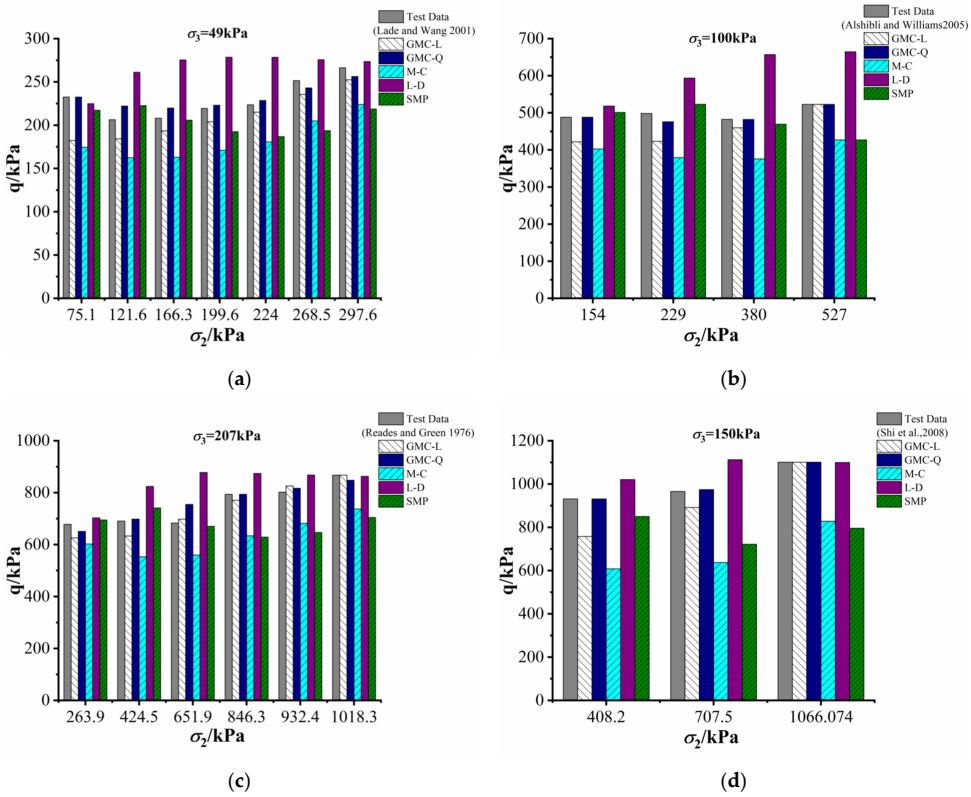


Figure 12. Comparisons of deviatoric stress by failure criteria and test data of soils (**a**) Santa Sand [37]; (**b**) Ottawa Sand [36]; (**c**) Ham River Sand [35]; (**d**) Gravel [46].

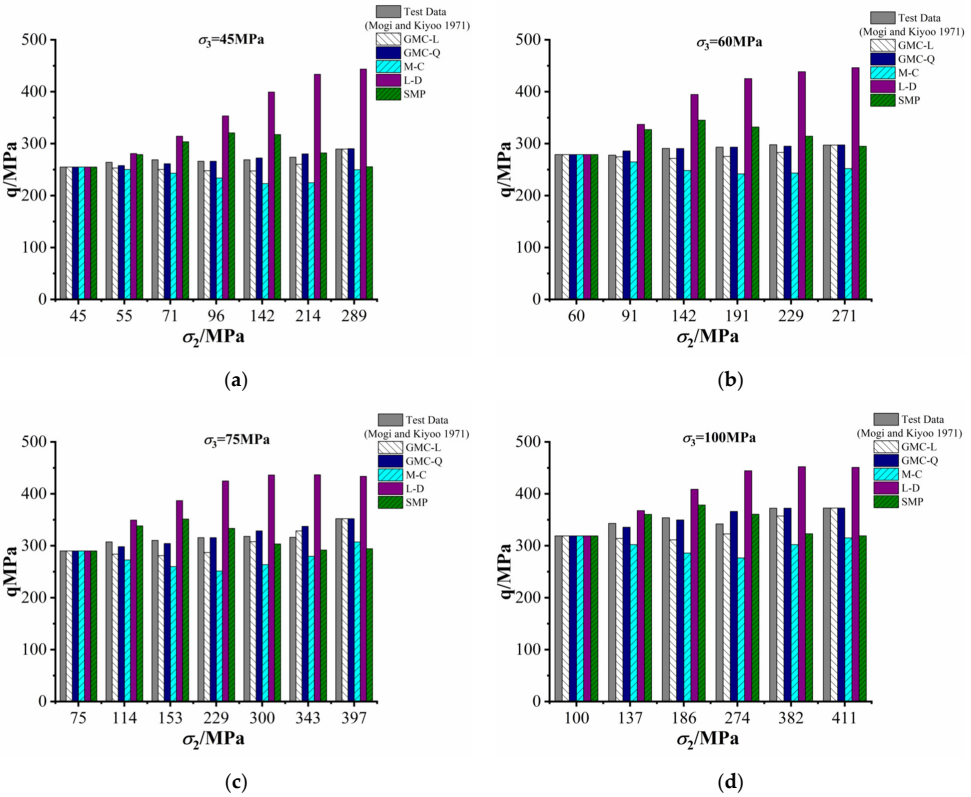


Figure 13. Comparisons of deviatoric stress evaluated by failure criteria and test data of Mizuho trachyte [40] (**a**) σ_3 = 45 MPa; (**b**) σ_3 = 60 MPa; (**c**) σ_3 = 75 MPa (σ_3 = 50 MPa); (**d**) σ_3 = 100 MPa.

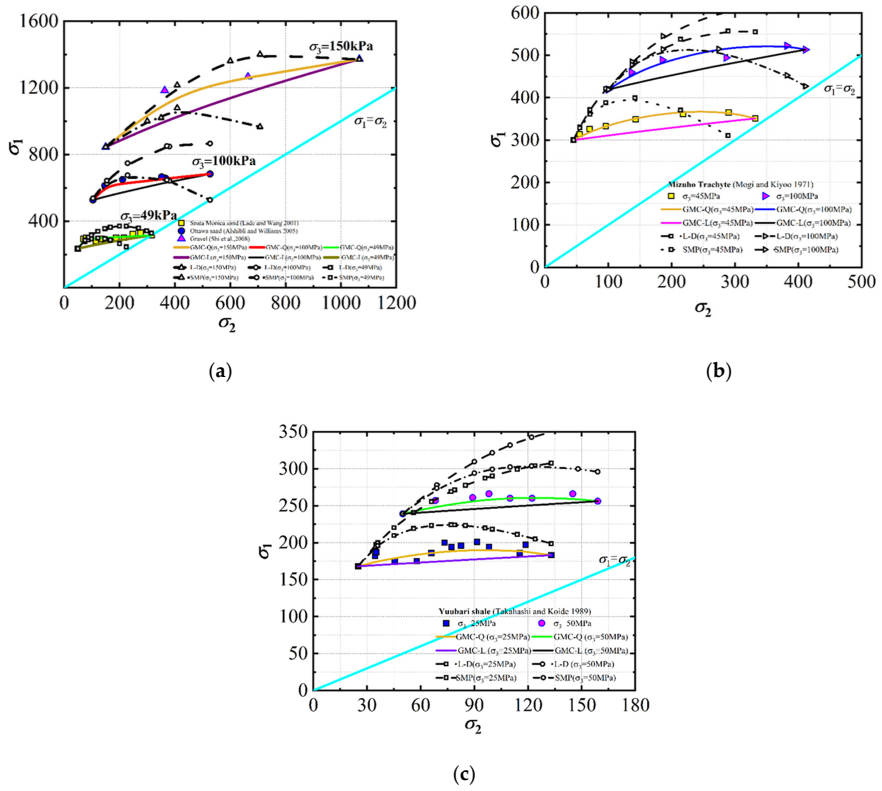


Figure 14. Comparisons of predictions of failure criteria with test data for various soils and rocks (**a**) Geotechnical materials [36,37,46]; (**b**) Mizuho trachyte [40]; (**c**) Yuubari shale [41].

7. Conclusions

By simply regarding the strength parameters c and ϕ in the conventional Mohr-Coulomb failure criterion as functions of the coefficient b of the intermediate principal stress, written as $c(b)$ and ϕ (b), respectively, the generalized Mohr-Coulomb failure creation, abbreviated as GMC, is derived. Numerous comparisons with well-established failure criteria, such as Lade–Duncan and SMP, indicate that GMC exhibits superior performance.

In the simplest way, the GMC can be built by just using a piece of conventional triaxial apparatus, if the true triaxial tests are not applicable. Even so, the GMC still matches test data better than either Lade–Duncan or SMP.

The Mohr-Coulomb criterion tends to overestimate shear deformation, while the Lade–Duncan criterion tends to underestimate shear deformation.

Even for an isotropic geomaterial, the failure surface in the stress space has been proved non-smooth per se.

Author Contributions: Conceptualization, D.T. and H.Z.; methodology, D.T. and H.Z.; validation, D.T. and H.Z.; writing—original draft, D.T.; writing—review and editing, D.T. and H.Z.; Funding acquisition, H.Z. All authors have read and agreed to the published version of the manuscript.

Funding: This research was funded by the National Natural Science Foundation of China, grant number 52130905 and 52079002.

Institutional Review Board Statement: Not applicable.

Informed Consent Statement: Not applicable.

Data Availability Statement: Not applicable.

Conflicts of Interest: The authors declare no conflict of interest.

Abbreviations

M-C	Mohr-Coulomb
GMC	Generalized Mohr-Coulomb
L-D	Lade–Duncan
SMP	Spatially Mobilized Plane
GMC-L	The GMC criterion is based on linear Lagrange interpolation
GMC-Q	The GMC criterion is based on quadric Lagrange interpolation

References

1. Taylor, D.W. *Fundamentals of Soil Mechanics*; Chapman and Hall: New York, NY, USA, 1948.
2. Wood, D.M. *Soil Behaviour and Critical State Soil Mechanics*; Cambridge University Press: Cambridge, UK, 2007.
3. Tomobe, H.; Fujisawa, K.; Murakami, A. A Mohr-Coulomb-Vilar model for constitutive relationship in root-soil interface under changing suction. *Soils Found* **2021**, *61*, 815–835. [CrossRef]
4. Ignat, R.; Baker, S.; Holmén, M.; Larsson, S. Triaxial extension and tension tests on lime-cement-improved clay. *Soils Found* **2019**, *59*, 1399–1416. [CrossRef]
5. Maghool, F.; Arulrajah, A.; Suksiripattanapong, C.; Horpibulsuk, S.; Mohajerani, A. Geotechnical properties of steel slag aggregates: Shear strength and stiffness. *Soils Found* **2019**, *59*, 1591–1601. [CrossRef]
6. Zheng, H. A three-dimensional rigorous method for stability analysis of landslides. *Eng. Geol.* **2012**, *145*, 30–40. [CrossRef]
7. Li, X.; Zhao, S.; He, S.; Yan, Q.; Lei, X. Seismic stability analysis of gravity retaining wall supporting c–φ soil with cracks. *Soils Found* **2019**, *59*, 1103–1111. [CrossRef]
8. Smith, G.N.; Smith, I.G.N. *Elements of Soil Mechanics*; Blackwell Science: Oxford, UK, 1998.
9. Lade, P.V.; Duncan, J.M. Elastoplastic stress-strain theory for cohesionless soil. *J. Geotech. Eng. Div.* **1975**, *101*, 1037–1053. [CrossRef]
10. Matsuoka, H.; Nakai, T. Stress-deformation and strength characteristics of soil under three different principal stresses. *Proc. Jpn. Soc. Civ. Eng.* **1974**, *232*, 59–70. [CrossRef]
11. Zheng, H.; Zhang, T.; Wang, Q. The mixed complementarity problem arising from non-associative plasticity with non-smooth yield surfaces. *Comput. Method Appl. M* **2020**, *361*, 112756. [CrossRef]
12. Zheng, H.; Chen, Q. Dimension extending technique for constitutive integration of plasticity with hardening–softening behaviors. *Comput. Method Appl. M* **2022**, *394*, 114833. [CrossRef]
13. Zienkiewicz, O.C.; Pande, G.N. Some useful forms of isotropic yield surfaces for soil and rock mechanics. In *Finite Elements in Geomechanics*; Gudehus, G., Ed.; Wiley: New York, NY, USA, 1977.
14. Menetrey, P.; Willam, K.J. Triaxial failure criterion for concrete and its generalization. *Struct. J.* **1995**, *92*, 311–318. [CrossRef]
15. Hoek, E.; Brown, E.T. Empirical strength criterion for rock masses. *J. Geotech. Eng. Div.* **1980**, *106*, 1013–1035. [CrossRef]
16. Yang, X.; Yin, J. Upper bound solution for ultimate bearing capacity with a modified Hoek–Brown failure criterion. *Int. J. Rock Mech. Min.* **2005**, *42*, 550–560. [CrossRef]
17. Luo, T.; Yao, Y.P.; Hou, W. *Soil Constitutive Models*; China Communications Press: Beijing, China, 2010. (In Chinese)
18. You, M. True-triaxial strength criteria for rock. *Int. J. Rock Mech. Min.* **2009**, *46*, 115–127. [CrossRef]
19. Liao, M.; Lai, Y.; Wang, C. A strength criterion for frozen sodium sulfate saline soil. *Can. Geotech. J.* **2016**, *53*, 1176–1185. [CrossRef]
20. Meyer, J.P.; Labuz, J.F. Linear failure criteria with three principal stresses. *Int. J. Rock Mech. Min.* **2013**, *60*, 180–187. [CrossRef]
21. Gao, F.; Yang, Y.; Cheng, H.; Cai, C. Novel 3D failure criterion for rock materials. *Int. J. Geomech.* **2019**, *19*, 4019046. [CrossRef]
22. Li, C.; Li, C.; Zhao, R.; Zhou, L. A strength criterion for rocks. *Mech. Mater.* **2021**, *154*, 103721. [CrossRef]
23. Liu, X.; Liu, E.; Song, B.; Wang, P. New twin-shear unified strength criterion. *Géotechnique Lett.* **2020**, *10*, 231–241. [CrossRef]
24. Yu, M.; Zan, Y.; Zhao, J.; Yoshimine, M. A unified strength criterion for rock material. *Int. J. Rock Mech. Min.* **2002**, *39*, 975–989. [CrossRef]
25. Lu, D. A constitutive model for soils considering stress paths based on generalized nonlinear strength theory. *Chin. J. Rock Mech. Eng.* **2007**, *26*, 1512. (In Chinese) [CrossRef]
26. Benz, T.; Schwab, R.; Kauther, R.A.; Vermeer, P.A. A Hoek–Brown criterion with intrinsic material strength factorization. *Int. J. Rock Mech. Min.* **2008**, *45*, 210–222. [CrossRef]
27. Priest, S. Three-dimensional failure criteria based on the Hoek–Brown criterion. *Rock Mech. Rock Eng.* **2012**, *45*, 989–993. [CrossRef]
28. Labuz, J.F.; Zang, A. Mohr-Coulomb failure criterion. *Rock Mech. Rock Eng.* **2012**, *45*, 975–979. [CrossRef]
29. Davis, R.O.; Selvadurai, A.R.S. *Plasticity and Geomechanics*; Cambridge University Press: Cambridge, UK, 2002.
30. Chen, W.F. *Constitutive Equations for Concrete and Soil*; China Architecture & Building Press: Beijing, China, 2005. (In Chinese)
31. Zheng, H.; Tham, L.G. Improved Bell's method for the stability analysis of slopes. *Int. J. Numer. Anal. Met.* **2009**, *33*, 1673–1689. [CrossRef]
32. Zheng, H.; Liu, D.F.; Li, C.G. Slope stability analysis based on elasto-plastic finite element method. *Int. J. Numer. Meth. Eng.* **2005**, *64*, 1871–1888. [CrossRef]
33. Zheng, H.; Liu, D.F.; Lee, C.F.; Tham, L.G. Displacement-controlled method and its applications to material non-linearity. *Int. J. Numer. Anal. Met.* **2005**, *29*, 209–226. [CrossRef]

34. Pressley, A.N. *Elementary Differential Geometry*; Springer Science & Business Media: Berlin/Heidelberg, Germany, 2010.
35. Reades, D.W.; Green, G.E. Independent stress control and triaxial extension tests on sand. *Géotechnique* **1976**, *26*, 551–576. [CrossRef]
36. Alshibli, K.A.; Williams, H.S. A true triaxial apparatus for soil testing with mixed boundary conditions. *Geotech. Test J.* **2005**, *28*, 534–543. [CrossRef]
37. Lade, P.V.; Wang, Q. Analysis of shear banding in true triaxial tests on sand. *J. Eng. Mech.* **2001**, *127*, 762–768. [CrossRef]
38. Hu, P.; Huang, M.S.; Ma, S.K.; Lv, X.L. True triaxial tests and strength characteristics of silty sand. *Rock Soil Mech.* **2011**, *32*, 465–470. (In Chinese) [CrossRef]
39. Jiang, J.S.; Cheng, Z.L.; Zuo, Y.Z.; Ding, H.S. Experimental investigation on strength characteristic of coarse-grained materials in three-dimensional stress state. *Rock Soil Mech.* **2018**, *39*, 3581–3588. (In Chinese) [CrossRef]
40. Mogi, K. Fracture and flow of rocks under high triaxial compression. *J. Geophys. Res.* **1971**, *76*, 1255–1269. [CrossRef]
41. Takahashi, M.; Koide, H. Effect of the intermediate principal stress on strength and deformation behavior of sedimentary rocks at the depth shallower than 2000 m. In Proceedings of the ISRM International Symposium: OnePetro, Pau, France, 30 August 1989.
42. Haimson, B.; Chang, C. A new true triaxial cell for testing mechanical properties of rock, and its use to determine rock strength and deformability of Westerly granite. *Int. J. Rock Mech. Min.* **2000**, *37*, 285–296. [CrossRef]
43. Craig, R.F. *Soil Mechanics*; E & FN Spon: London, UK, 1997.
44. Rosales Garzón, S.E.; Hanna, A.M. Critical-state shear strength and pore pressure of granular materials. *Int. J. Geomech.* **2021**, *21*, 4021237. [CrossRef]
45. Sutherland, H.B.; Mesdary, M.S. The influence of the intermediate principal stress on the strength of sand. In Proceedings of the 7th International Conference on Soil Mechanics and Foundation Engineering, Mexico City, Mexico, 1 January 1969; Sociedad Mexicana de Mecanica. pp. 391–399.
46. Shi, W.C. True Triaxial Tests on Coarse-Grained Soils and Study on Constitutive Model. Ph.D. Thesis, Hohai University, Nanjing, China, 2008. (In Chinese).
47. Ma, X.; Haimson, B.C. Failure characteristics of two porous sandstones subjected to true triaxial stresses. *J. Geophys. Res. Solid Earth* **2016**, *121*, 6477–6498. [CrossRef]
48. Chang, C.; Haimson, B. True triaxial strength and deformability of the German Continental Deep Drilling Program (KTB) deep hole amphibolite. *J. Geophys. Res. Solid Earth* **2000**, *105*, 18999–19013. [CrossRef]
49. Liu, X. Study on the True Triaxial Tests and Strength Characteristics of the Q_3 Loess. Master Thesis, Chang'an University, Xi'an, China, 2014. (In Chinese).

Disclaimer/Publisher's Note: The statements, opinions and data contained in all publications are solely those of the individual author(s) and contributor(s) and not of MDPI and/or the editor(s). MDPI and/or the editor(s) disclaim responsibility for any injury to people or property resulting from any ideas, methods, instructions or products referred to in the content.